

## **ALTERNATIVE SUB-DOMAIN MOMENT METHODS FOR ANALYZING THIN-WIRE CIRCULAR LOOPS**

**P. J. Papakanellos**

School of Electrical and Computer Engineering  
National Technical University of Athens  
GR 157-73 Zografou, Athens, Greece

**Abstract**—An alternative sub-domain formulation is presented, in two variants, for the analysis of thin-wire circular loops via moment methods. Curved piecewise sinusoids are used as basis functions, while both point matching and reaction matching (Galerkin's method) are examined as testing schemes. The present study is primarily focused on frill-driven loops, but some of the essential similarities and differences between them and gap-driven ones are also discussed in brief. Numerical results are presented to verify the two variants of the proposed formulation and demonstrate their capabilities for analyzing small and large loops. Special attention is drawn to the behavior of the solutions as the number of basis/testing functions grows. Finally, a complexity analysis is attempted and the potential savings in execution times that may be attained by taking advantage of certain features of the proposed numerical schemes are discussed.

### **1. INTRODUCTION**

Thin-wire loops are perhaps the most widely spread antennas after straight cylindrical dipoles. Because of this fact and the geometrical simplicity of circular loops, these have been the topic of many theoretical studies; see, for example, [1–4] and certain references provided therein. Most of the analytical works on this subject are based on Fourier expansions for the unknown loop current, whose coefficients (weights of the associated trigonometric modes) are expressed in closed form with the aid of integrals of nontrivial functions (namely, modified Bessel and Lommel-Weber functions), which are difficult to deal with and are practically useful only for moderately small loops. Alternatively, curved thin-wire antennas can be studied numerically via moment methods [5]; advances on this subject can be found in [6, 7] and

certain works cited therein. Entire-domain formulations with periodic basis functions seem to be suitable for loop antennas; however, their applicability is restricted to a few wavelengths in circumference [8]. In contrast, sub-domain formulations seem to be capable of analyzing arbitrarily large loops [9, 10].

In this paper, a sub-domain formulation is presented for the analysis of thin-wire circular loops via moment methods. The proposed formulation is alternative in the sense that it results from first principles, without utilizing any *a priori* knowledge in the form of an integral equation for the unknown loop current. In the same sense, the proposed formulation is innately direct and, at least in principle, readily adaptable to more complex geometries. The formulation is directly derived by enforcing the boundary condition of the tangential electric field on the surface of the loop, after simply expanding the radiated electromagnetic (EM) field as a weighted superposition (with unknown coefficients) of the EM fields excited by properly selected sub-domain basis functions. These latter fields are analytically expressed in the form of simple integrals arising from the magnetic vector potentials of the basis functions. A simple collocation technique and Galerkin’s method are adopted, in order to form matrix equations for the unknown expansion weights. In both cases, the loop current is obtained from the basis functions lying on the wire axis; thus, the approach of this paper is conceptually similar to that of the well-known approximate (non-singular) kernel for straight cylindrical dipoles, which also arises from the assumption of an “equivalent” axial current.

In principle, the use of non-singular kernels in thin-wire analysis has serious implications. It has been shown that the integral equations for the current on straight cylindrical dipoles of finite length (namely, Hallén’s and Pocklington’s equations) are non-solvable when the exact kernel involved is replaced by the approximate (non-singular) one, at least for an excitation field of a delta-gap source, a plane wave, or a frill generator [11–14]. This fact is behind certain difficulties that usually arise when applying moment methods to thin-wire antennas and scatterers, the most evident of which is the appearance of oscillations in the computed current distributions for quite large numbers of basis functions. These oscillations are not due to round-off errors and, thus, cannot be overcome by using more powerful computers. At least for sub-domain basis functions, and irrespective of which of the aforementioned excitations is assumed, oscillations seem to originate from the wire ends and tend to cover the whole current distribution as the number of basis functions grows; similar oscillations also occur in the imaginary part of the current near the driving point of gap-driven antennas. As far as frill-driven loops are concerned, previous studies

via sub-domain moment methods with non-singular kernels have not brought out similar oscillations (see, for example, [10, 15]). This fact could be intuitively anticipated for curved frill-driven wire antennas without open ends, on the basis of the behavior of the oscillations that accompany frill-driven wire antennas with open ends [13]. This lack of oscillations can be also perceived by analogy to the case of the frill-fed cylindrical dipole of infinite length studied in [13, 16]. On the contrary, oscillations are expected to occur near the driving point of gap-driven loops, in light of the analytical study of gap-driven cylindrical dipoles of infinite length in [11] (see also [16]). A detailed study of the solvability of certain integral equations with non-singular kernels for thin-wire circular loops is presented in [17].

In this paper, particular attention is drawn to the solutions as the number of basis functions grows, in order to examine the behavior of the results and isolate the effects of round-off and quadrature errors, which typically impose certain difficulties to numerical methods that are based on non-singular kernels. Representative numerical results are presented for frill-driven circular loops of small and large circumference, together with a few comments for gap-driven ones. Moderately small loops are examined first, in order to delve into the behavior of the solutions as the number of basis functions increases, as well as to validate the results through comparison with those of other methods. Larger loops are subsequently examined and relevant results are presented to demonstrate some of the essential features of the proposed numerical schemes. Finally, a complexity analysis is outlined and general guidelines are provided for the efficient implementation of these schemes.

## 2. FORMULATION

### 2.1. Description of the Problem

The geometry under study consists in a circular loop of radius  $b$  (or total arc length  $L = 2\pi b$ ), which is constructed from a perfectly conducting wire of radius  $a$ . The loop lies on the  $z = 0$  plane of the concentric coordinates system shown in Fig. 1. The wire is thin in the sense that  $a \ll b$  and  $a \ll \lambda$ , where  $\lambda$  is the operating wavelength; therefore, the associated surface current density is assumed to be longitudinally directed (that is,  $\phi$ -directed) and invariant around the wire's cross-section. The loop is driven by the magnetic frill generator described in [4], which is located at  $\phi = 0$ , as shown in Fig. 1. In fact, the geometry described so far simulates a half-loop antenna that is coaxially fed through a perfectly conducting ground plane. The inner and outer conductor radii of the coaxial cable are  $a$  and  $a_f$ , respectively.

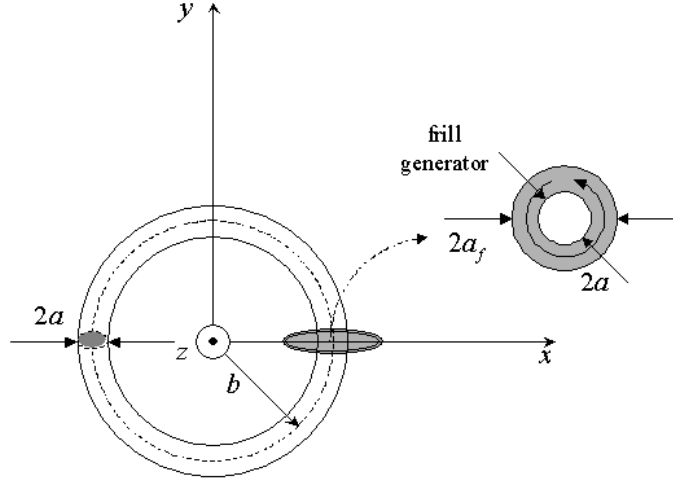


**Figure 1.** Geometry of a circular loop excited by a frill source.

## 2.2. Formulation for Frill-driven Loops

In what follows, the time convention  $\exp(j\omega t)$  is assumed and suppressed. The unknown EM field radiated by the loop is attributed to a longitudinal filamentary current  $I(\phi)$  (defined at  $\rho = b$  and  $z = 0$ ), which is expressed as a weighted superposition of  $2N$  sub-domain basis functions

$$I(\phi) \approx \sum_{n=1}^{2N} w_n f_n(\phi). \quad (1)$$

The number of basis functions is assumed to be even for convenience; nonetheless, the formulation that follows is readily adaptable to odd numbers of basis functions. The basis functions  $f_n(\phi)$  are selected to be piecewise sinusoids of curvature radius  $b$  and angular width  $2\delta = 2\pi/N$  (or, equivalently, arc length  $2\delta b$ ), which are expressed as

$$f_n(\phi) = \begin{cases} \sin[k_0 b(\delta - |\phi - \phi_n|)], & |\phi - \phi_n| \leq \delta \\ 0, & |\phi - \phi_n| > \delta \end{cases} \quad n = 1, 2, \dots, 2N, \quad (2)$$

where  $k_0 = 2\pi/\lambda$  and  $\phi_n = (n - 1)\delta$ .

For the derivation of the unknown expansion weights  $w_n$ , the boundary condition of the tangential electric field is directly enforced by equating the  $\phi$ -directed component of the radiated electric field, which is expressed as superposition of the fields excited by the basis

functions of (2) (see Appendix A), to the negative of the corresponding component of the excitation field. In cases of straight wires, cylindrical symmetry holds with respect to the wire axis and, thus, the associated boundary condition can be enforced along any line on the surface of the wire. On the other hand, when the wire is curved, cylindrical symmetry with respect to the wire axis does not hold anymore. For thin-wire loops, it seems quite reasonable to expect that the solutions are rather insensitive to where one enforces the boundary condition, as long as  $b \pm a \approx b$ ; nevertheless, discrepancies of order at least up to 10% were observed in the input admittances resulting from the method proposed in [9, 10] by shifting the matching points from the outer points ( $\rho = b + a$ ,  $z = 0$ ) to the upper/lower ( $\rho = b$ ,  $z = \pm a$ ) or inner ones ( $\rho = b - a$ ,  $z = 0$ ). From these checks, it was also found that the enforcement of the boundary condition at the upper/lower points yields moderate results, which are very close to the mean value resulting by shifting the testing line around the wire's transversal periphery. Because of this fact, the boundary condition is enforced along the circular ring defined by  $\rho = b$  and  $z = a$ , yielding

$$\sum_{n=1}^{2N} w_n \left[ \hat{\phi} \cdot \vec{E}_n(b, \phi, a) \right] = -\hat{\phi} \cdot \vec{E}_f(b, \phi, a) \quad (3)$$

where  $\vec{E}_n$  stands for the electric field excited by the current of (2), which can be computed using the results in Appendix A, and  $\vec{E}_f$  denotes the electric field of the frill source.

A computationally simple algorithm can be formed on the basis of a point-matching (PM) strategy. This is accomplished by directly enforcing (3) at  $2N$  points that are located at  $(b, \phi_m, a)$ . Alternatively, one can reach the same result by replacing the testing functions below with the shifted delta functions  $\delta(\phi - \phi_m)$ .

According to Galerkin's method, (3) is matched following a reaction-matching (RM) strategy; this consists in multiplying both sides of (3) by  $f_m(\phi)$  (testing functions) and integrating over the corresponding angular intervals. This leads to a  $2N \times 2N$  system of equations, which is written as

$$\sum_{n=1}^{2N} Z_{n,m} w_n = -V_m, \quad m = 1, 2, \dots, 2N, \quad (4)$$

where

$$Z_{n,m} = - \int_{\phi_m - \delta}^{\phi_m + \delta} \left[ \hat{\phi} \cdot \vec{E}_n(b, \phi, a) \right] f_m(\phi) b d\phi, \quad (5)$$

$$V_m = - \int_{\phi_m - \delta}^{\phi_m + \delta} \left[ \hat{\phi} \cdot \vec{E}_f(b, \phi, a) \right] f_m(\phi) b d\phi. \quad (6)$$

Due to symmetry, the reaction integrals in (5) depend on  $|n - m|$  only, not on  $n$  and  $m$  separately. Hence, the system of (4) can be constructed swiftly by utilizing the equality  $Z_{n,m} = Z_{|n-m|+1,1}$ . The voltage terms in (6) involve the tangential component of the excitation electric field, which is given by an integral over a toroidal difference angle  $\chi$  and possesses a singularity arising for  $\chi \rightarrow 0$  and  $\phi \rightarrow 0$  (for explicit expressions, see (8)–(13) in [4]). In order to facilitate the relevant computations, this integral can be simplified by utilizing an approximate expression for the distance between two points on the surface of the loop, as suggested and exploited in [10]. In particular, the electric field of the frill generator can be expressed as

$$\hat{\phi} \cdot \vec{E}_f(\phi) \approx - \frac{V_f \cos \phi}{\ln \left( \frac{a_f}{a} \right)} \left\{ \frac{\exp \left[ -jk_0 \sqrt{a_f^2 + 2b^2(1 - \cos \phi)} \right]}{\sqrt{a_f^2 + 2b^2(1 - \cos \phi)}} - \frac{\exp \left[ -jk_0 \sqrt{a^2 + 2b^2(1 - \cos \phi)} \right]}{\sqrt{a^2 + 2b^2(1 - \cos \phi)}} \right\}, \quad (7)$$

where  $V_f$  is the equivalent feeding voltage of the frill source. For convenience, the feeding voltage is taken to be 1 V.

It is worth stressing that the PM variant of the proposed formulation can be considered as an implementation of the method of auxiliary sources (MAS) [18] with axially located auxiliary sources of piecewise sinusoidal currents (instead of elementary ones that are usually assumed within the context of the MAS). The critical point underlying this resemblance is the assumption of the axial current of (1), which is also linked to the use of the approximate kernel in thin-wire analysis (for relevant discussions, see [19, 20]).

### 2.3. Modification for Delta-gap Excitation

The delta-gap source is perhaps the most frequently used feeding model in thin-wire antenna modeling. Nevertheless, it is associated with an infinite capacitance arising across the infinitesimal gap, a fact that may lead to several problems. From a theoretical point of view, this infinite capacitance is tantamount to the diverging imaginary part of the input current (input susceptance). Formulations that are based on the approximate kernel may demonstrate even worse behavior, since they lead to solutions that oscillate near the feeding gap [11–14, 16, 17].

For these reasons, the delta-gap source was not chosen as the excitation type of primary interest in this paper.

The formulation provided for the frill source can be readily adapted to virtually any excitation field; for the delta-gap source, the only modification needed is limited to the voltage terms of (6), which are now derived by replacing  $-\vec{E}_f$  with the electric field of the delta-gap source. The opposite sign is an outcome of the fact that the electric field of the delta-function generator is maintained as a scalar potential difference  $V_g$  across the gap, whereas the frill generator produces an external excitation field impinging upon the surface of the loop. The excitation vector associated with the delta-gap generator has only one nonzero term. In the PM case, this term is simply  $V_1 = -V_g\pi/N$ . In the RM case, the integration in (6) leads to  $V_1 = -V_g \sin(k_0 b\pi/N)$ .

### 3. NUMERICAL RESULTS

Thin-wire moment methods with non-singular kernels are typically highly vulnerable to round-off and other numerical errors, like those accompanying quadrature routines. In particular, the associated matrix equations usually exhibit rapidly growing condition numbers with the number of basis/testing functions [11, 13, 14]. For this reason, the accuracy of the computations was thoroughly examined by applying quadrature rules of varying order and independent system solvers [21]. The numerical results that follow were obtained using double-precision arithmetic and were found to be virtually unaffected by numerical errors.

First, numerical results are presented to validate the proposed schemes and to delve into the behavior of the numerical solutions as  $N$  grows. For this purpose, results for the input admittance as  $N$  is increased are depicted in Fig. 2 for a loop antenna with  $b/\lambda = 0.2$ ,  $a/\lambda = 0.005$  and  $a_f/a = 2.3$  (corresponding to an air-filled coaxial line of characteristic impedance  $50\Omega$ ). For the purpose of comparison, results derived by applying the method of [10] are also shown. Apparently, for  $N > 100$ , all three data sets shown in Fig. 2 are in excellent agreement. By contrast, there exist notable differences in the behavior of the solutions for smaller  $N$  (note that certain results for small  $N$  are out of scale). Specifically, the RM results are much less dispersed in comparison with both the PM and the reference ones, which are stabilized for notably larger  $N$ ; namely, for  $N$  close to the parameter  $L/(2a) = \pi b/a$  (loop length to diameter ratio), which is equivalent to choosing the arc-length spacing between adjacent basis/testing functions  $\delta$  roughly equal to the wire radius  $a$ . From numerous tests, it was found that this behavior is indicative of

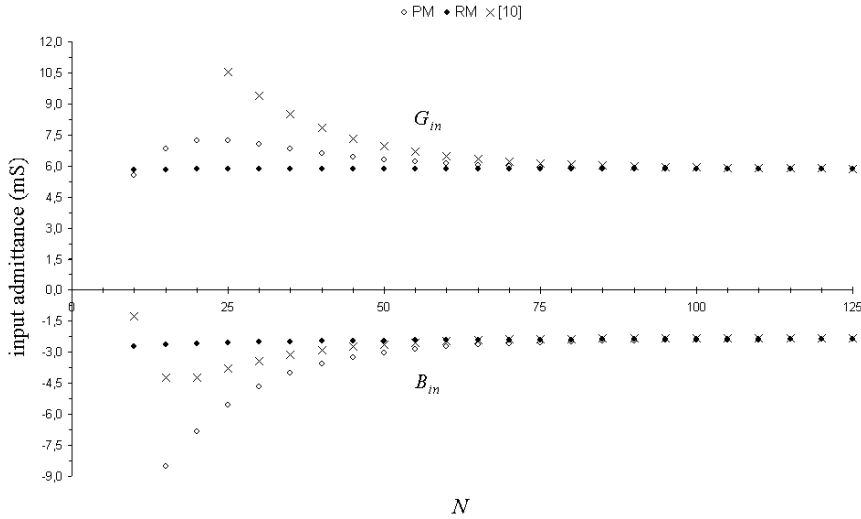


**Figure 2.** Computed values for the input admittance of a frill-driven loop as  $N$  grows, for  $b/\lambda = 0.2$ ,  $a/\lambda = 0.005$  and  $a_f/a = 2.3$ .

what should be anticipated in general (that is, for small and large loops). This assertion is further reinforced by the numerical results in [9]; for example, as reported therein, stable results (regarding the computed input conductance) for loops with  $a/\lambda = 0.01$  and  $k_0b = 10$ , 25, 50 and 100 were obtained for 600, 2500, 5000 and 8000 expansion terms, respectively, quite close to what is expected according to the aforementioned rough rule (note that the number of basis/testing functions is denoted by  $N$  in [9, 10], but equals  $2N$  here). Apart from the differences in the computed driving-point admittances for moderately small  $N$ , other less evident discrepancies among different solutions also exist. As a representative example, Fig. 3 depicts the magnitude of the total tangential electric field, normalized to the peak intensity of the driving field, along the testing ring on the surface of the loop of Fig. 2 for  $N = 75$ . By definition, the quantity illustrated in Fig. 3 provides a measure for the error in the boundary condition of (3). Obviously, the PM error curve exhibits an oscillatory behavior with regular (equidistant) deep nulls at the locations of the matching points and sharp peaks near the midpoints, whereas the RM error curve is smoother, though still oscillatory, with less steep minima and lower peaks.

To further explore the behavior of the solutions, selected results

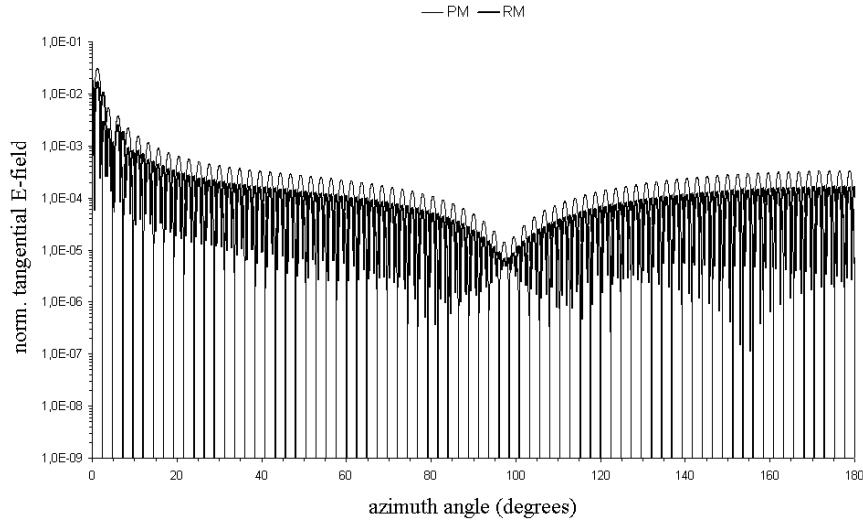


**Figure 3.** Plot of the magnitude of the normalized tangential electric field on a frill-driven loop with  $b/\lambda = 0.2$ ,  $a/\lambda = 0.005$  and  $a_f/a = 2.3$ , for  $N = 75$ .

for the input admittance as a function of  $b$  are provided in Figs. 4 (PM) and 5 (RM) for  $0.15 \leq b/\lambda \leq 0.50$ ,  $\alpha/\lambda = 0.005$  and  $a_f/a = 2.3$ . The legends “high” and “low” denote high and low discretization levels, which correspond to  $N = \lceil \pi b/a \rceil$  and  $N = \lceil \pi b/(4a) \rceil$ , respectively, where  $\lceil \bullet \rceil$  is the roundup operator. As expected from Fig. 2, the curves depicted in Fig. 5 are in very close mutual agreement, whereas significant differences are lucid in Fig. 4. Obviously, these differences do not increase in magnitude as  $b$  becomes larger, a fact that further manifests the importance of the ratio of  $N$  to the parameter  $\pi b/a$ . For  $N$  close to this parameter, both the PM/RM results were found to be in excellent agreement with independent numerical results obtained from the method of [10] and quite close to experimental data provided in [4].

With regard to the possible occurrence of oscillations in the resulting current distributions, certain checks have verified the findings of [17]. In particular, oscillations that are not due to round-off errors were not observed in the currents of frill-driven loops. By contrast, numerous tests have revealed the appearance of oscillations in the imaginary part of the computed current near the driving point of gap-driven loops. These oscillations first appear as  $N$  grows and reaches (or roughly exceeds)  $\pi b/a$ . To illustrate this behavior, Fig. 6 depicts

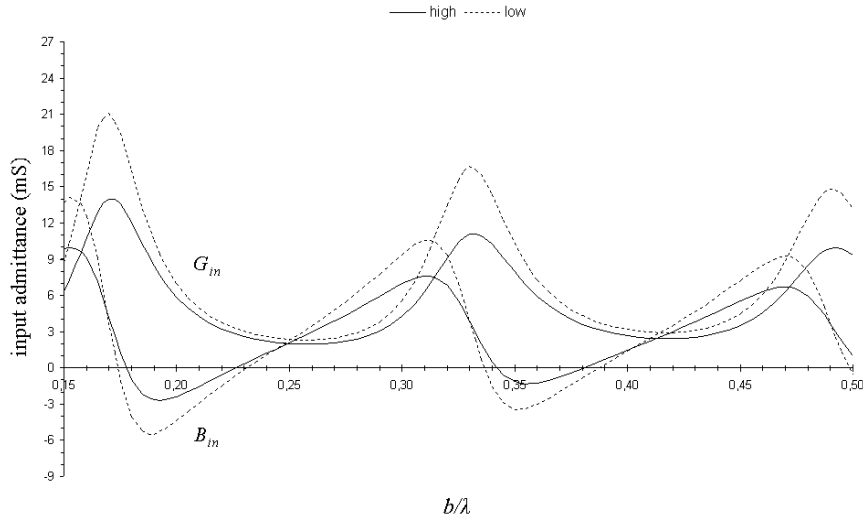


**Figure 4.** Plot of the input admittance of a frill-driven loop as a function of  $b/\lambda$ , as derived by the PM scheme, for  $0.15 \leq b/\lambda \leq 0.50$ ,  $a/\lambda = 0.005$  and  $a_f/a = 2.3$ . High and low discretization levels correspond to  $N = \lceil \pi b/a \rceil$  and  $N = \lceil \pi b/(4a) \rceil$ , respectively.

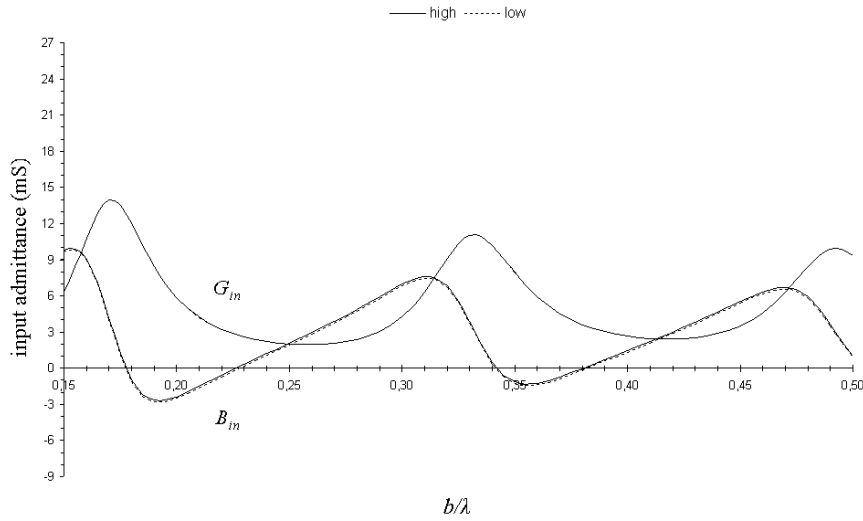


**Figure 5.** Plot of the input admittance of a frill-driven loop as a function of  $b/\lambda$ , as derived by the RM scheme, for  $0.15 \leq b/\lambda \leq 0.50$ ,  $a/\lambda = 0.005$  and  $a_f/a = 2.3$ . High and low discretization levels correspond to  $N = \lceil \pi b/a \rceil$  and  $N = \lceil \pi b/(4a) \rceil$ , respectively.

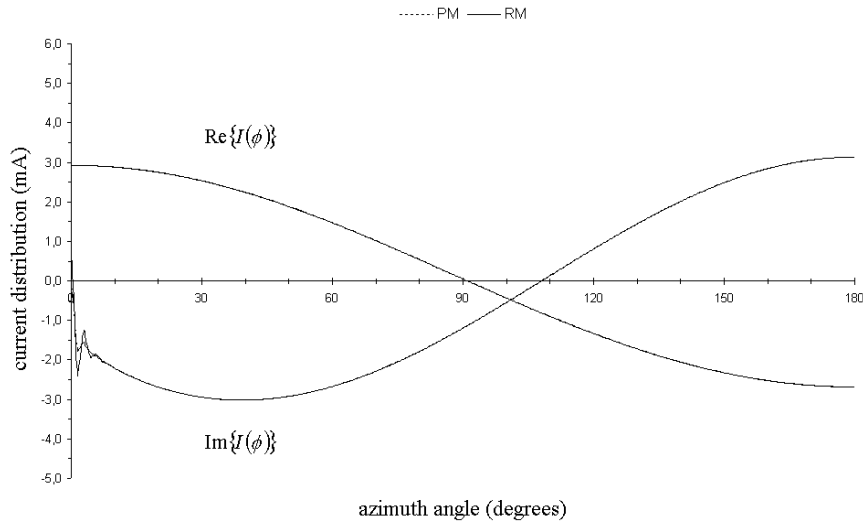


**Figure 6.** Computed current distribution on a loop with  $b/\lambda = 0.2$  and  $a/\lambda = 0.005$ , when excited by a delta-gap generator, for  $N = 125$ .

the computed current distribution for  $b/\lambda = 0.2$ ,  $a/\lambda = 0.005$  and  $N = 125$ . Further increase in  $N$  yields more rapid oscillations, before matrix ill-conditioning effects begin to dominate. As far as the choice of  $N$  is concerned, one should bear in mind that the oscillating behavior of the resulting currents is restrictive in cases of gap-driven loops, for which  $N$  should be smaller than  $\pi b/a$ . However, in cases of frill-driven loops, the situation is quite different and  $N$  can be increased beyond  $\pi b/a$ .

Sub-domain moment methods seem to be applicable to arbitrarily large loops [9, 10]. Indeed, apart from the increasing computational workload, there is no major restriction on the applicability of these methods to large loops, with the possible exceptions of the numerical errors accumulated when trying to solve quite large systems (for which a large number of arithmetic operations is required) and the underflow errors in the computation of weak interactions between distant elements that may occur when attempting to analyze exuberantly large loops. The former can be detected by applying different system solvers. In the event of the latter, meaningful results could be obtained by neglecting any interactions that are weaker than a carefully selected threshold. With double-precision arithmetic, the developed codes exhibited no need for such a threshold, at least for circumferences up to those considered in [9, 10]. In particular, numerous tests revealed

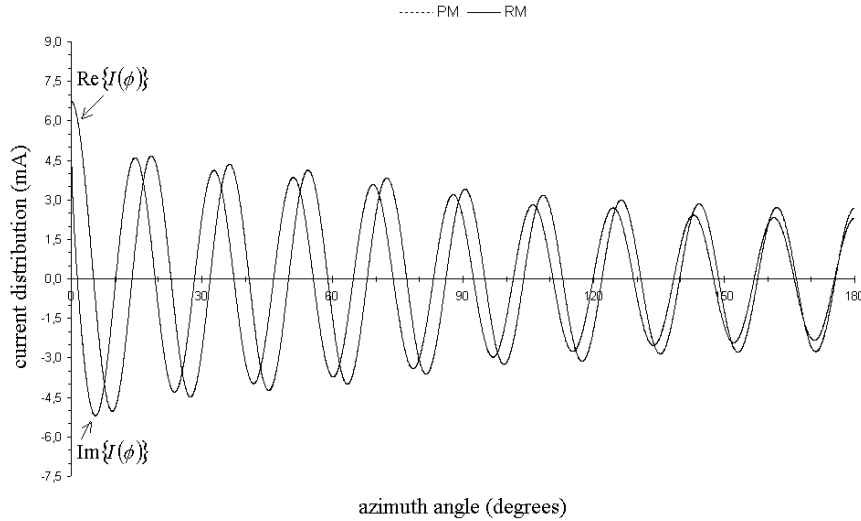


**Figure 7.** Computed current distribution on a loop with  $k_0b = 20$  and  $a/\lambda = 0.01$ , when excited by a frill generator with  $a_f/a = 2.3$ , for  $N = 1000$ .

excellent agreement with Fig. 11 in [9] and Fig. 3 in [10]. As an example, Fig. 7 depicts the current distribution on a frill-driven loop with  $k_0b = 20$  ( $b/\lambda \approx 3.183$ ),  $a/\lambda = 0.01$  and  $a_f/a = 2.3$ . Apparently, there is no distinguishable difference between PM and RM curves. Excellent agreement was also observed between the results of Fig. 7 and the currents obtained from the method of [10].

#### 4. COMPLEXITY ANALYSIS

The benefits of Galerkin's method against collocation techniques are, as usual, reaped at the expense of greater complexity in forming the associated matrix equations. Indeed, for given  $N$ , the matrix-filling procedure is much more time-consuming in the RM case. However, this fact by itself cannot justify the superiority of the PM strategy against the RM one in terms of any possible efficiency metric, since the former reaches stable results for notably larger  $N$ . Although relatively unimportant when utilizing fast system solvers that exploit the special structure of the interaction matrix (symmetric Toeplitz), this feature of the RM scheme could lead to notable savings when such solvers are either not available or not applicable; for example, in cases of deformed (noncircular) loops or coupled loops, which yield interaction matrices

that are not Toeplitz. In such cases, the time spent by the system solver tends to dominate the matrix-filling time as  $N$  grows. Thus, for large-scale problems and conventional solvers whose operations are of order  $O(N^3)$ , the RM scheme may be more efficient in comparison with the PM one. In order to carry out *a priori* comparisons, one has to quantify the associated computational cost in the form of functions of the critical parameters that determine the numbers of complex operations<sup>†</sup> involved in the procedures for the formation and solution of (4) [22]. For the LU solver of [21] (which has been modified for treating complex matrices) and a  $G$ -point Gauss-Legendre quadrature routine, the cost functions were roughly approximated as

$$C_{\text{PM}} \approx 2N_{\text{PM}}(50G+19) + \frac{2(2N_{\text{PM}})^3 + 15(2N_{\text{PM}})^2 + 13(2N_{\text{PM}})}{3}, \quad (8)$$

$$C_{\text{RM}} \approx 2N_{\text{RM}}(100G^2 + 50G + 2) + \frac{2(2N_{\text{RM}})^3 + 15(2N_{\text{RM}})^2 + 13(2N_{\text{RM}})}{3}, \quad (9)$$

where  $2N_{\text{PM}}$  and  $2N_{\text{RM}}$  are the respective total numbers of unknowns. The expressions of (8) and (9) can be utilized in different ways. For instance, for a given geometry and for sufficiently large  $G$  to ensure the accuracy of the computations, one can set  $N_{\text{RM}} = \kappa N_{\text{PM}}$  (as already remarked, useful results are typically obtained for  $N_{\text{PM}}$  close to  $\pi b/a$ ) and proceed to determine the range of  $\kappa$  for which  $C_{\text{RM}} \leq C_{\text{PM}}$ . On the other hand, for a given  $\kappa < 1$  (note that useful results can be obtained for  $N_{\text{RM}} \approx \kappa\pi b/a$  with  $\kappa$  as small as 0.25), the cost functions of (8) and (9) can be used to decide whether the RM scheme should be preferred over the PM one or not. In order to conduct a systematic parametric study, the inequality  $C_{\text{PM}} - C_{\text{RM}} \geq 0$  can be solved with  $N_{\text{RM}} = \kappa N_{\text{PM}}$ , in order to obtain the range of  $N_{\text{PM}}$  over which the inequality holds. Elementary algebraic manipulation yields two nonzero roots of the equality  $C_{\text{PM}} - C_{\text{RM}} = 0$ , which are expressed as

$$2N_{\pm} = \frac{-P_1 \pm \sqrt{P_1^2 - 4P_0P_2}}{2P_2}, \quad (10)$$

where  $P_0 = -100G^2\kappa - 50G(\kappa - 1) + (70 - 19\kappa)/3$ ,  $P_1 = 5(1 - \kappa^2)$  and  $P_2 = 2(1 - \kappa^3)/3$ . For  $\kappa < 1$ , both  $P_1$  and  $P_2$  are positive, whereas  $P_0$

---

<sup>†</sup> The number of complex operations should not be confused with the number of complex multiplications, as long as other elementary operations (such as complex additions) may require comparable times for their execution. The cost functions of this paper were derived from the total numbers of elementary workload “units” associated with the complex additions/multiplications and elementary functions calculations required by the developed codes in a Visual C++ programming environment.

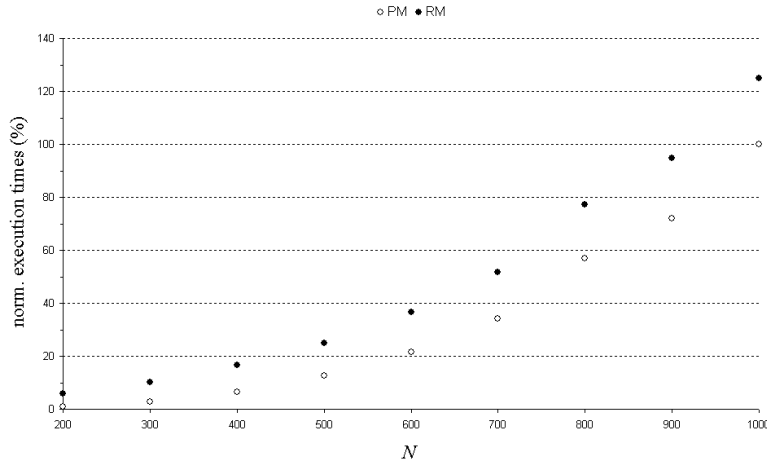


**Figure 8.** Normalized execution times for a frill-driven loop with  $k_0 b = 20$ ,  $a/\lambda = 0.01$  and  $a_f/a = 2.3$ .

is negative when

$$G > \frac{1 - \kappa}{4\kappa} + \frac{\sqrt{75 + 130\kappa - \kappa^2}}{20\sqrt{3}\kappa}. \quad (11)$$

Within the interval  $0.1 \leq \kappa < 1$ , this latter condition is satisfied even for  $G$  as small as 5 and, thus, the roots given by (10) are real numbers with  $N_+ > 0$  and  $N_- < 0$ . In such cases, the inequality  $C_{\text{PM}} - C_{\text{RM}} > 0$  holds when  $N > N_+$ . As a direct outcome, the RM scheme is expected to be more efficient than the PM one for  $\pi b/a$  larger than  $N_+$ .

In order to verify the findings of the last paragraph, several tests were conducted. As an example, results for the large loop of Fig. 7 (for which  $\pi b/a = 1000$ ) are provided. Measured execution times, normalized to that required by the PM code for  $N = 1000$ , are shown in Fig. 8 for  $G = 64$ . From (8) and (9), it can be readily deduced that the RM scheme is expected to be more efficient than the PM one for  $\kappa < 0.949$ . As it is apparent from Fig. 8, savings in the execution times are indeed attained even for  $\kappa$  as large as 0.9, as anticipated.

## 5. CONCLUDING REMARKS AND POSSIBLE EXTENSIONS

A direct sub-domain formulation was presented for analyzing thin-wire circular loops via moment methods. The proposed formulation

was developed in two variants by adopting both point-matching and reaction-matching testing schemes. Numerical results were presented to verify the computations and provide some insight into the behavior of the resulting solutions as  $N$  grows.

Sub-domain formulations are capable of analyzing thin-wire loops of arbitrary circumference. In cases of circular loops, the associated interaction matrices are typically symmetric Toeplitz ones, which are amenable to fast system solvers of low complexity. In such cases, overall efficient computer codes can be constructed for coping with large circular loops. Nonetheless, in cases of deformed loops or coupled loops, the interaction matrices are not symmetric Toeplitz ones. In such cases, important savings in the computational workload could be achieved by applying the proposed RM scheme for a moderately small number of unknowns, as demonstrated for the “benchmark” case of a large circular loop.

## ACKNOWLEDGMENT

The author wishes to express his appreciation to Dr. H. T. Anastassiou and Dr. G. Fikioris for their constructive discussions and comments. This work was conducted as part of a post-doc research program supported by the State Scholarships Foundation of Greece.

## APPENDIX A.

Analytic expressions for the vector potentials and near fields of circular filaments with uniform/trigonometric currents are available in the open literature [23–25]. However, the expressions in [23–25] are valid only for closed circular filaments; thus, they cannot be used for the sub-domain basis functions of (2), for which a direct approach is followed hereinafter.

For convenience, a curved filamentary segment of radius  $b$  and known current  $f(\phi)$  is assumed, which is situated on the  $z = 0$  plane and spans the angular interval between  $\phi^-$  and  $\phi^+$ . Then, the associated magnetic vector potential  $\vec{A} = A_\rho \hat{\rho} + A_\phi \hat{\phi}$  is given by

$$A_\rho(\rho, \phi, z) = \frac{\mu_0}{4\pi} \int_{\phi^-}^{\phi^+} \sin(\phi - \phi') \frac{e^{-jk_0 R}}{R} f(\phi') b d\phi', \quad (\text{A1})$$

$$A_\phi(\rho, \phi, z) = \frac{\mu_0}{4\pi} \int_{\phi^-}^{\phi^+} \cos(\phi - \phi') \frac{e^{-jk_0 R}}{R} f(\phi') b d\phi', \quad (\text{A2})$$

where  $\mu_0 = 4\pi \times 10^{-7}$  H/m and  $R$  is the distance from the source point

$(b, \phi', 0)$  to the observation point  $(\rho, \phi, z)$ , which is given by

$$R = \sqrt{\rho^2 + b^2 - 2\rho b \cos(\phi - \phi') + z^2} \quad (\text{A3})$$

Expressions for the radiated EM field can be derived from

$$\vec{H} = \frac{1}{\mu_0} \nabla \times \vec{A}, \quad (\text{A4})$$

$$\vec{E} = -j \frac{\zeta_0}{k_0} \nabla \times \vec{H}, \quad (\text{A5})$$

where  $\zeta_0 = 120\pi \Omega$ . By substituting (A1) and (A2) into (A4), explicit expressions for the magnetic field are obtained, which are given by

$$H_\rho(\rho, \phi, z) = \frac{1}{4\pi} \int_{\phi^-}^{\phi^+} z \cos(\phi - \phi') \frac{1 + jk_0 R}{R^2} \frac{e^{-jk_0 R}}{R} f(\phi') b d\phi', \quad (\text{A6})$$

$$H_\phi(\rho, \phi, z) = -\frac{1}{4\pi} \int_{\phi^-}^{\phi^+} z \sin(\phi - \phi') \frac{1 + jk_0 R}{R^2} \frac{e^{-jk_0 R}}{R} f(\phi') b d\phi', \quad (\text{A7})$$

$$H_z(\rho, \phi, z) = \frac{1}{4\pi} \int_{\phi^-}^{\phi^+} [b - \rho \cos(\phi - \phi')] \frac{1 + jk_0 R}{R^2} \frac{e^{-jk_0 R}}{R} f(\phi') b d\phi'. \quad (\text{A8})$$

Using these expressions, one may obtain the electric field from (A5). For example, the longitudinal component of the electric field, which is involved in the formulation presented in the main body of the paper, is

$$E_\phi(\rho, \phi, z) = -j \frac{\zeta_0}{4\pi k_0} \int_{\phi^-}^{\phi^+} F_\phi(\rho, \phi - \phi', z) \frac{e^{-jk_0 R}}{R} f(\phi') b d\phi', \quad (\text{A9})$$

where

$$F_\phi(\rho, \phi - \phi', z) = \frac{(k_0 R)^2 - (1 + jk_0 R)}{R^2} \cos(\phi - \phi') + \rho b \frac{3(1 + jk_0 R) - (k_0 R)^2}{R^4} \sin^2(\phi - \phi'). \quad (\text{A10})$$

Finally, explicit expressions for the electric and magnetic fields of the basis functions of (2) can be derived by substituting  $\phi^\pm \rightarrow \phi_n \pm \delta$  (or, equivalently,  $\phi^\pm \rightarrow \phi_{n\pm 1}$ ) and  $f(\phi') \rightarrow f_n(\phi')$ .

## REFERENCES

1. Wu, T. T., "Theory of the thin circular loop antenna," *Journal of Mathematical Physics*, Vol. 3, No. 6, 1301–1304, 1962.

2. King, R. W. P., "The loop antenna for transmission and reception," *Antenna Theory*, R. E. Collin and F. J. Zucker (eds.), Ch. 11, McGraw-Hill, New York, 1969.
3. King, R. W. P. and C. W. Harrison, *Antennas and Waves: A Modern Approach*, Ch. 9, M.I.T. Press, Cambridge, MA, 1969.
4. Zhou, G. and G. S. Smith, "An accurate theoretical model for the thin-wire circular half-loop antenna," *IEEE Transactions on Antennas and Propagation*, Vol. 39, No. 8, 1167–1177, 1991.
5. Harrington, R. F., *Field Computation by Moment Methods*, MacMillan, New York, 1968.
6. Champagne II, N. J., J. T. Williams, and D. R. Wilton, "The use of curved segments for numerically modeling thin wire antennas and scatterers," *IEEE Transactions on Antennas and Propagation*, Vol. 40, No. 6, 682–689, 1992.
7. Rogers, S. D. and C. M. Butler, "An efficient curved-wire integral equation solution technique," *IEEE Transactions on Antennas and Propagation*, Vol. 49, No. 1, 70–79, 2001.
8. Li, L.-W., C.-P. Lim, and M.-S. Leong, "Method-of-moments analysis of electrically large circular-loop antennas: Nonuniform currents," *IEE Proceedings on Microwaves, Antennas and Propagation*, Vol. 146, No. 6, 416–420, 1999.
9. Anastassiou, H. T., "Fast, simple and accurate computation of the currents on an arbitrarily large circular loop antenna," *IEEE Transactions on Antennas and Propagation*, Vol. 54, No. 3, 860–866, 2006.
10. Anastassiou, H. T., "An efficient algorithm for the input susceptance of an arbitrarily large, circular loop antenna," *Electronics Letters*, Vol. 42, No. 16, 897–898, 2006.
11. Fikioris, G. and T. T. Wu, "On the application of numerical methods to Hallén's equation," *IEEE Transactions on Antennas and Propagation*, Vol. 49, No. 3, 383–392, 2001.
12. Fikioris, G., "The approximate integral equation for a cylindrical scatterer has no solution," *Journal of Electromagnetic Waves and Applications*, Vol. 15, No. 9, 1153–1159, 2001.
13. Fikioris, G., J. Lionas, and C. G. Lioutas, "The use of the frill generator in thin-wire integral equations," *IEEE Transactions on Antennas and Propagation*, Vol. 51, No. 8, 1847–1854, 2003.
14. King, R. W. P., G. J. Fikioris, and R. B. Mack, *Cylindrical Antennas and Arrays*, Chs. 1 and 13, Cambridge University Press, Cambridge, MA, 2002.
15. Jensen, M. A. and Y. Rahmat-Samii, "Electromagnetic character-

- istics of superquadric wire loop antennas,” *IEEE Transactions on Antennas and Propagation*, Vol. 42, No. 2, 264–269, 1994.
16. Fikioris, G. and C. A. Valagiannopoulos, “Input admittances arising from explicit solutions to integral equations for infinite-length dipole antennas,” *Progress In Electromagnetics Research*, PIER 55, 285–306, 2005.
  17. Fikioris, G., P. J. Papakanellos, and H. T. Anastassiou, “On the use of nonsingular kernels in certain integral equations for thin-wire circular-loop antennas,” submitted to *IEEE Transactions on Antennas and Propagation*.
  18. Kaklamani, D. I. and H. T. Anastassiou, “Aspects of the method of auxiliary sources (MAS) in computational electromagnetics,” *IEEE Antennas and Propagation Magazine*, Vol. 44, No. 3, 48–64, 2002.
  19. Papakanellos, P. J. and C. N. Capsalis, “On the combination of the method of auxiliary sources with reaction matching for the analysis of thin cylindrical antennas,” *International Journal of Numerical Modeling*, Vol. 17, No. 5, 433–449, 2004.
  20. Fikioris, G., “On two types of convergence in the method of auxiliary sources,” *IEEE Transactions on Antennas and Propagation*, Vol. 54, No. 7, 2022–2033, 2006.
  21. Press, W. H., S. A. Teukolsky, W. T. Vetterling, and B. P. Flannery, *Numerical Recipes in C*, Chs. 2 and 4, Cambridge University Press, New York, 1992.
  22. Avdikos, G. K. and H. T. Anastassiou, “Computational cost estimations and comparisons for three methods of applied electromagnetics,” *IEEE Antennas and Propagation Magazine*, Vol. 47, No. 1, 121–129, 2005.
  23. Werner, D. H., “An exact integration procedure for vector potentials of thin circular loop antennas,” *IEEE Transactions on Antennas and Propagation*, Vol. 44, No. 2, 157–165, 1996.
  24. Overfelt, P. L., “Near fields of the constant current thin circular loop antenna of arbitrary radius,” *IEEE Transactions on Antennas and Propagation*, Vol. 44, No. 2, 166–171, 1996.
  25. Li, L.-W., M.-S. Leong, P.-S. Kooi, and T.-S. Yeo, “Exact solutions of electromagnetic fields in both near and far zones radiated by thin circular-loop antennas: A general representation,” *IEEE Transactions on Antennas and Propagation*, Vol. 45, No. 12, 1741–1748, 1997.